JOURNAL OF COMPUTATIONAL PHYSICS 85, 417–433 (1989)

A Numerical Method for the Calculation of the Diffusion of High Energy Electrons in a Heterogeneous Medium

P. STORCHI AND R. J. VAN DER LINDEN*

Dr. Daniel den Hoed Cancer Center, Groene Hilledijk 301, 3075 EA Rotterdam, The Netherlands

Received July 1, 1987; revised December 20, 1988

A numerical method is presented for the calculation of the diffusion of high energy electrons in a heterogeneous medium. It forms a numerical solution to Fermi's diffusion equation for multiple Coulomb scattering. This equation is used in the simulation applications of electron beams. This method approximates the directional distribution of the electrons by a Gaussian function multiplied by a linear combination of the corresponding Hermite polynomials.

1. INTRODUCTION

For the calculation of the absorbed dose in clinical applications of electron beams, the most popular methods are based on the convolution of pencil beams [1, 2]. The spatial distribution needed in the convolution procedure can be derived from measurements, from Monte Carlo calculations, or from analytical calculations. Measurements of the distribution of very thin electron beams were performed by Lax [3]. Monte Carlo calculation of the diffusion of pencil beams in a homogeneous medium were performed by Andreo and Brahme [4] and Berger and Seltzer [5]. An analytical expression based on a theoretical model of Fermi for multiple Coulomb scattering was given by Rossi and Greisen [6] for the case in which the energy of the electrons remains constant. Later this expression was generalized by Eyges [7] for the case in which the energy decreases with the depth z.

This Fermi–Eyges theory gives a rough description of the total scattering process only. For instance, it does not take into account large angle scattering and secondary electrons and uses implicitly the approximation $\operatorname{tg}\theta \simeq \theta$. Nevertheless, the analytical expression given by this theory has been successfully applied in the pencil beam method for the prediction of dose distribution in a patient [8, 9]. The pencil beam method can be split into two parts. One part is the calculation of the energy decrease; the other part is the calculation of the diffusion due to multiple scattering in the medium. This paper is dedicated to the second part: the diffusion due to multiple scattering in a heterogeneous medium.

* Present address: Technical University of Delft, Department of Physics, Lorenzweg 1, Delft, The Netherlands.

0021-9991/89 $3.00

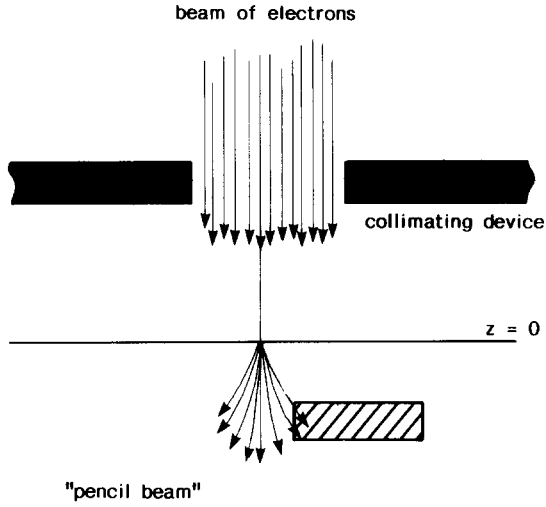

FIG. 1. A broad beam of electrons can be understood as a collection of ray beams. Each ray beam becomes broader in the medium as a result of scattering and forms a so-called pencil beam. In the medium the electron flux distribution is then computed by convolution of these pencil beams over the field defined by the collimating device. A strong limitation of this "pencil beam method" is that a pencil beam whose axis does not cross a block of different material, as depicted in the figure, will not be influenced by this block. If its axis crosses the block then the pencil beam "sees" it as an infinite slab.

In the pencil method a slab-geometry is assumed for each pencil beam; i.e., each individual pencil beam diffuses in the material along its axis. Thus, for example, the pencil beam shown in Fig. 1 will not "see" the block of different material. However, in clinical practice the slab-geometry cannot be assumed. This explains the differences between calculation and measurement as reported in [10–12]. To avoid this restriction, a numerical method has been developed by Storchi and Huizenga [13] to solve directly the equation of Fermi, as described in [6, 7], for a broad beam. This method uses the first three directional moments of the electron distribution at each point in the medium. In this paper a mathematical generalization of that method will be given for an arbitrary number of moments. Here too, only the scattering part will be considered. In order to give some introductory information, the theory of Fermi and the pencil beam solution will be reviewed briefly in the next section.

2. FERMI THEORY AND SOLUTION OF THE PENCIL BEAM FOR THE SLAB-GEOMETRY

The Fermi theory for the diffusion of electrons in a medium has been described by Rossi and Greisen [6]. The assumption of the model is resumed in the equation

$$F(z+\delta, r, \omega) = \int_{\Omega} F(z, r-\delta\omega, \omega')\, \rho_{\delta}(\omega' \to \omega)\, d\omega' + O(\delta^2), \tag{1}$$

where F is the distribution (planar fluence) of the electrons as a function of depth z, lateral position $r=(x, y)$ and direction $\omega=(\theta_x, \theta_y)$. θ_x and θ_y are the projected angles [6] and Ω denotes the space of all values of ω. $O(\delta^2)$ is an unknown term of order δ^2. $\rho_\delta(\omega' \to \omega)$ is the scattering function that describes the multiple scattering of the electrons in a slab of thickness δ.

Rossi and Greisen did not use an explicit expression for ρ_δ but defined it by its first three moments,

$$\int_\Omega \rho_\delta \, d\omega = 1 \tag{2}$$

$$\int_\Omega \rho_\delta \omega \, d\omega = 0 \tag{3}$$

$$\int_\Omega \rho_\delta \omega^2 \, d\omega = T\delta, \tag{4}$$

where T is the linear angular scattering power ($\text{rad}^2\,\text{cm}^{-1}$) [14]. T is defined as the increase of the variance of the directional (or angular) distribution of a thin, near mono-directional beam crossing a unit slab of material. T depends on the kind of material and on the energy of the electrons.

Using in (1) a Taylor expansion relative to ω and r and Eqs. (2), (3), and (4) and decreasing δ to zero, we get

$$\frac{\partial F}{\partial z} = -\theta_x \frac{\partial F}{\partial x} - \theta_y \frac{\partial F}{\partial y} + \frac{T}{4}\left(\frac{\partial^2 F}{\partial x^2} + \frac{\partial^2 F}{\partial y^2}\right). \tag{5}$$

In the case of a slab-geometry and with some simplification with respect to the energy, the scattering power T depends on the depth z only. In this case the solution of (5) has been given by Eyges [7] for a point mono-directional source

$$F(z, x, y, \theta_x, \theta_y) = F(z, x, \theta_x)\, F(z, y, \theta_y) \tag{6}$$

$$F(z, x, \theta_x) = \frac{1}{(2\pi(A_0 A_1 - A_2^2))^{1/2}} \exp\left\{-\frac{A_0 x^2 + 2A_1 x\theta_x + A_2\theta_x^2}{2(A_0 A_1 - A_2^2)}\right\}, \tag{7}$$

where

$$A_i(z) = \frac{1}{2}\int_0^z T(z')(z-z')^i \, dz', \qquad i=0, 1, 2. \tag{8}$$

In the case of a broad beam and a medium with slab-geometry the solution of (5) can be found by the convolution of Eq. (7) [15, 13], but this method is not valid in the case of arbitrary heterogeneities. In the next sections, a numerical approximation to the solution of (5) for an arbitrary heterogeneous medium will be presented. For simplification of the formula we will only consider cases where the distribution

of the electrons is not dependent on y, i.e., when the beam is very large in the y-direction and when the heterogeneity structures do not depend on y. The extension of the method to the 3-dimensional case will be explained briefly in Appendix C.

3. Numerical Solution

Although Eq. (1) has been used as the starting point in the derivation of the expression of the pencil beam for a slab-geometry, it can be applied also to the general case of a broad beam and an arbitrary heterogeneous medium. To obtain a numerical calculation scheme in the 2-dimensional case, we return to Eq. (1) and neglect the term $O(\delta^2)$,

$$F(z+\delta, x, \theta) = \int_{-\infty}^{+\infty} F(z, x-\delta\theta, \theta')\, \rho_\delta(\theta' \to \theta)\, d\theta', \tag{9}$$

where θ is used for θ_x for simplification of the notation.

For the scattering term we will use the explicit form

$$\rho_\delta(\theta' \to \theta) = \frac{1}{\sqrt{\pi T\delta}} \exp\left\{-\frac{(\theta-\theta')^2}{T\delta}\right\}. \tag{10}$$

The first algorithm, given in [13], computes the distribution F at discrete depths z_i and discrete points x_j. It uses the first three directional moments,

$$F_i = \int_{-\infty}^{+\infty} \theta^i F(z, x, \theta)\, d\theta, \qquad i = 0, 1, 2, \tag{11}$$

to approximate the distribution as a function of the direction with

$$F(z, x, \theta) = \frac{F_0}{\sqrt{2\pi\sigma^2}} \exp\left\{-\frac{(\theta-\bar{\theta})^2}{2\sigma^2}\right\} = F_0(z, x)\, G(\theta; \bar{\theta}, \sigma^2), \tag{12}$$

where $F_0(z, x)$ is the planar fluence,

$$\bar{\theta} = F_1(z, x)/F_0(z, x) \tag{13}$$

is the mean direction,

$$\sigma^2 = F_2(z, x)/F_0(z, x) - \bar{\theta}^2 \tag{14}$$

is the mean square deviation, and

$$G(\theta; \bar{\theta}, \sigma^2) = \frac{1}{\sqrt{2\pi\sigma^2}} \exp\left\{-\frac{(\theta-\bar{\theta})^2}{2\sigma^2}\right\}. \tag{15}$$

As pointed out in [13] the use of only three moments does not in all cases approximate the solution of (5) to a satisfactory accuracy. In order to use

n moments, where $n > 3$, the distribution as a function of the direction will be approximated by a sum of shifted Hermite polynomials $\hat{H}_k(\theta; \bar{\theta}, \sigma^2)$ weighted by the corresponding Gaussian function $G(\theta; \bar{\theta}, \sigma^2)$,

$$F(z, x, \theta) = \sum_{k=0}^{n} a_k \hat{H}_k(\theta; \bar{\theta}, \sigma^2)\, G(\theta; \bar{\theta}, \sigma^2), \tag{16}$$

where a_k, $\bar{\theta}$, and σ^2 are functions of z and x. Because of the choice of $\bar{\theta}$ and σ^2, the parameters a_1 and a_2 are equal to zero as will be seen later. For $n = 2$ Eq. (16) reduces to (12). The definition and properties of the shifted Hermite polynomials $\hat{H}_k$, which are very similar to those of the normal Hermite polynomials, are given in Appendix A.

The distribution at depth $z + \delta$ is computed from the distribution at depth z by performing the convolution in Eq. (9) and by computing the new moments at depth $z + \delta$. Substituting (10) and (16) into (9) yields

$$\tilde{F}(z + \delta, x, \theta) = \sum_{k=0}^{n} a_k(z, x - \delta\theta) \int_{-\infty}^{+\infty} \hat{H}_k(\theta; \bar{\theta}, \sigma^2)\, G(\theta; \bar{\theta}, \sigma^2)\, G\left(\theta - \theta'; 0, \frac{1}{2}\delta T\right) d\theta'. \tag{17}$$

The new symbol $\tilde{F}$ is used to point out that expression (17) cannot be exactly written in the desired form (16). In order to evaluate (17) further, the convolution of $\hat{H}_k(\theta; \bar{\theta}, \sigma^2)\, G(\theta; \bar{\theta}, \sigma^2)$ by $G(\theta; 0, \frac{1}{2}\delta T)$ is computed by Fourier transform and the result is substituted into (17), giving

$$\tilde{F}(z + \delta, x, \theta) = \left[\sum_{k=0}^{n} a_k \hat{H}_k\left(\theta; \bar{\theta}, \sigma^2 + \frac{1}{2}\delta T\right) G\left(\theta; \bar{\theta}, \sigma^2 + \frac{1}{2}\delta T\right) \right]_{z, x - \delta\theta}. \tag{18}$$

The moments at depth $z + \delta$ are computed from Eq. (18),

$$\begin{aligned} \tilde{F}_i(z + \delta, x) &= \int_{-\infty}^{+\infty} \theta^i F(z + \delta, x, \theta)\, d\theta \\ &= \int_{-\infty}^{+\infty} \theta^i \sum_{k=0}^{n} a_k \hat{H}_k\left(\theta; \bar{\theta}, \sigma^2 + \frac{1}{2}\delta T\right) G\left(\theta; \bar{\theta}, \sigma^2 + \frac{1}{2}\delta T\right) d\theta, \end{aligned} \tag{19}$$

where it must be kept in mind that a_k, $\bar{\theta}$, and σ^2 in (19) are functions of $x - \delta\theta$ at depth z. The numerical evaluation of (19) will be discussed in Section 5.

Equation (19) gives the moments at depth $z + \delta$ computed from the coefficients a_k, $\bar{\theta}$, and σ^2 at depth z. The theorem given in the next section shows that the result of Eq. (19) can be used to find a new set of coefficients at depth $z + \delta$. We will now compute the new coefficients a_k, $\bar{\theta}$, and σ^2 at depth $z + \delta$. We first choose $\bar{\theta}(z + \delta, r)$ and $\sigma^2(z + \delta, r)$ as defined by Eq. (13) and (14). This implicitly fixes the function $G(\theta; \bar{\theta}, \sigma^2)$. Once this choice is made, the Fourier co-efficients of the series (16) can be computed from the moments (19) using the recursion relation derived in the next section,

$$F_i = \sum_{k=1}^{i} \frac{i!}{(i-k)!} G_{i-k} a_k, \tag{20}$$

where

$$G_i = \int_{-\infty}^{+\infty} \theta^i G(\theta; \bar{\theta}, \sigma^2)\, d\theta \tag{21}$$

is given in Appendix B. The values of the first five coefficients are

$$a_0 = F_0 \tag{22}$$

$$a_1 = a_2 = 0 \tag{23}$$

$$a_3 = \frac{(\sigma^2)^{3/2}}{3!} \gamma_1 \tag{24}$$

$$a_4 = \frac{(\sigma^2)^2}{4!} \gamma_2, \tag{25}$$

where γ_1 and γ_2 are respectively the skewness and the excess of the distribution $F(\theta)$.

In this way the coefficients a_k, $\bar{\theta}$, and σ^2 are calculated at depth $z+\delta$ and serve as input to the calculation at depth $z+2\delta$. Some aspects of the method outlined above will be discussed in the next two sections. Then some results will be highlighted.

4. Evaluation of the Recurrent Relation (20)

To derive the recursion relation (20), Eq. (16) is substituted into the definition of the moments (11), giving

$$F_i = \sum_{k=1}^{i} a_k \int_{-\infty}^{+\infty} \theta^i \hat{H}_k(\theta)\, G(\theta)\, d\theta + a_0 \int_{-\infty}^{+\infty} \theta^i G(\theta)\, d\theta. \tag{26}$$

Applying the recursion relation of the $\hat{H}_k$'s given in Appendix A and partial integration of the first term of (26) we find

$$\begin{aligned} F_i &= \sum_{k=1}^{i} a_k \int_{-\infty}^{+\infty} \theta^{i-1} \hat{H}_{k-1}(\theta)\, G(\theta)\, d\theta + a_0 \int_{-\infty}^{+\infty} \theta^i G(\theta)\, d\theta \\ &= \sum_{k=1}^{i-1} a_{k+1} \int_{-\infty}^{+\infty} \theta^{i-1} \hat{H}_k(\theta)\, G(\theta)\, d\theta + i a_1 \int_{-\infty}^{+\infty} \theta^{i-1} G(\theta)\, d\theta \\ &\quad + a_0 \int_{-\infty}^{+\infty} \theta^i G(\theta)\, d\theta. \end{aligned} \tag{27}$$

By repeated partial integration we find Eq. (20):

$$F_i = \sum_{k=1}^{i} \frac{i!}{(i-k)!} G_{i-k} a_k.$$

The next theorem makes a link between the moments given by the relation (19) and the a_k in the recurrent relation (20).

THEOREM. *Assume that the moments of the function* $\tilde{F}(\theta)$ *exist and that the development of* $\tilde{F}(\theta)/G(\theta; \bar{\theta}, \sigma^2)$ *in the Fourier series*

$$\tilde{F}(\theta)/G(\theta; \bar{\theta}, \sigma^2) = \sum_{k=0}^{\infty} a_k \hat{H}_k(\theta; \bar{\theta}, \sigma^2) \tag{28}$$

is valid; then $\tilde{F}(\theta)$ *and the approximation* $F(\theta)$ *given by the truncated series*

$$F(\theta) = \sum_{k=0}^{n} a_k \hat{H}_k(\theta; \bar{\theta}, \sigma^2)\, G(\theta; \bar{\theta}, \sigma^2) \tag{29}$$

have the same first n moments.

Let F_i and $\tilde{F}_i$ be the ith moments of $F(\theta)$ and $\tilde{F}(\theta)$, respectively. We remark that

$$\hat{H}_i(\theta) = \sum_{k=0}^{n} \alpha_{k,i} \theta^k, \tag{30}$$

where the $\alpha_{k,i}$ are co-efficients. Then we can deduce that

$$\begin{aligned} \sum_{k=0}^{i} \alpha_{k,i} F_k &= \int_{-\infty}^{+\infty} \hat{H}_i F \, d\theta = \sum_{k=0}^{n} a_k \int_{-\infty}^{+\infty} \hat{H}_k \hat{H}_i G \, d\theta \\ &= a_i \|\hat{H}_i\|^2 = \int_{-\infty}^{+\infty} \hat{H}_i \tilde{F} \, d\theta = \sum_{k=0}^{i} \alpha_{k,i} \tilde{F}_k. \end{aligned} \tag{31}$$

Thus

$$\sum_{k=0}^{i} \alpha_{k,i} (F_k - \tilde{F}_k) = 0, \qquad i \leqslant n \tag{32}$$

and the theorem follows.

5. Numerical Evaluation of the Moments

In the numerical implementation we consider a set of nodes $\{x_j, j = 1, ..., m\}$ such that we can assume F_0 to be zero for $x < x_1$ and $x > x_m$. These nodes are the centers of contiguous intervals $[x_j - \frac{1}{2}\delta_x, x_j + \frac{1}{2}\delta_x]$. In each interval the parameters

a_k, $\bar{\theta}$, and σ^2 are taken to be constant. In terms of these intervals the Eq. (22) can be written as

$$F_i(z+\delta, x) = \sum_{j=1}^{m} \int_{\theta_j(x)}^{\theta_{j+1}(x)} \sum_{k=0}^{n} \theta^i a_k \hat{H}_k(\theta; \bar{\theta}, \sigma^2)\, G(\theta; \bar{\theta}, \sigma^2)\, d\theta, \tag{33}$$

where

$$\theta_j(x) = \frac{x - x_j - \delta_x/2}{\delta} \tag{34a}$$

$$\theta_{j+1}(x) = \frac{x - x_j + \delta_x/2}{\delta} = \frac{x - x_{j+1} - \delta_x/2}{\delta}. \tag{34b}$$

Figure 2 depicts the situation for the calculation in node $x_{j'}$.

Because the parameters a_k, $\bar{\theta}$, and σ^2 are constant in the intervals $[\theta_j(x), \theta_{j+1}(x)]$ we get

$$F_i(z+\delta, x) = \sum_{j=1}^{m} \sum_{k=0}^{n} a_{k,j} [I_{i,k}(\theta_{j+1}(x); \bar{\theta}_j, \sigma_j^2) - I_{i,k}(\theta_j(x); \bar{\theta}_j, \sigma_j^2)], \tag{35}$$

where

$$I_{i,k}(a; \bar{\theta}, \sigma^2) = \int_0^a \theta^i \hat{H}_k(\theta; \bar{\theta}, \sigma^2)\, G(\theta; \bar{\theta}, \sigma^2)\, d\theta \tag{36}$$

is evaluated recursively in Appendix B.

To evaluate the coefficients in the interval $[x_j, -\frac{1}{2}\delta_x, x_j, +\frac{1}{2}\delta_x]$ at depth $z+\delta$

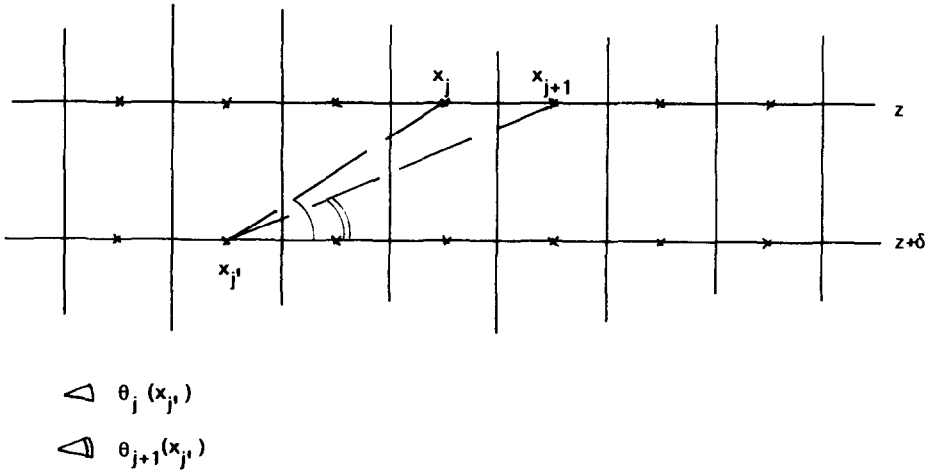

FIG. 2. Geometric description of the calculation mesh.

it would be possible to evaluate the F_i's only in the point $x_{j'}$, but experience has shown that in some situations the result is poor, for instance, in combination with field divergence. A good estimate of the moments is made by taking their means over the interval $[x_j, -\frac{1}{2}\delta_x, x_j, +\frac{1}{2}\delta_x]$ at depth $z+\delta$,

$$F_{i,j'}(z+\delta) = \int_{x_{j'}-\delta_x/2}^{x_{j'}+\delta_x/2} F_i(z+\delta, x)\,dx$$

$$= \sum_{j=1}^{m} \sum_{k=0}^{n} a_{k,j} \left[\int_{x_{j'}-\delta_x/2}^{x_{j'}+\delta_x/2} I_{i,k}(\theta_{j+1}(x); \bar{\theta}_j, \sigma_j^2)\,dx \right.$$

$$\left. - \int_{x_{j'}-\delta_x/2}^{x_{j'}+\delta_x/2} I_{i,k}(\theta_j(x); \bar{\theta}_j, \sigma_j^2)\,dx \right], \tag{37}$$

where the evaluation of $\int_{x_1}^{x_2} I_{i,k}(\theta(x); \bar{\theta}, \sigma^2)\,dx$ is also given in Appendix B.

6. Results

This numerical method has been implemented in a computer code (FORTRAN) running on a PDP-11/44 for a maximum of six moments ($n=5$). In this section some results will be presented.

Homogeneous Medium

The analytical solution $F(z, x, \theta_x)$ of Eq. (5), as well as its moments $F_0(z, x)$, $F_1(z, x)$, and $F_2(z, x)$, has been given in [13] for the case in which the scattering power T depends on z only. It has been shown [13] that already in the particular case of a constant T, the solution of (5) is not totally described by a Gaussian function. Figure 3 shows the parameters F_0 and σ^2 on the central axis of a parallel beam for a constant T. This case is not realistic from a physical point of view but it allows an easy comparison to the analytical solution of the Fermi–Eyges equation. In the case of the Gaussian approximation ($n=2$) the numerical curves obviously deviate from the analytical curves. These differences cannot be made smaller by decreasing the spatial step sizes. Adding two moments ($n=4$) clearly improves the result. It is expected that the numerical solution will converge toward the analytical solution; however, because of the limitation of the PDP-11/44, it was not possible to compute the solution for more moments. In this case $n=5$ does not further improve the result on the central axis because the odd moments of the symmetric distributions are zero.

Heterogeneous Medium

Figure 4 shows the planar fluence distribution of a broad parallel beam of width 10 cm crossing an air cavity of cross section 2×1 cm^2 at a depth of 1 cm in water. The initial energy of the electrons is 13 MeV. In the calculations, the scattering power T at the point (z, x) depends on the material and on the energy of the

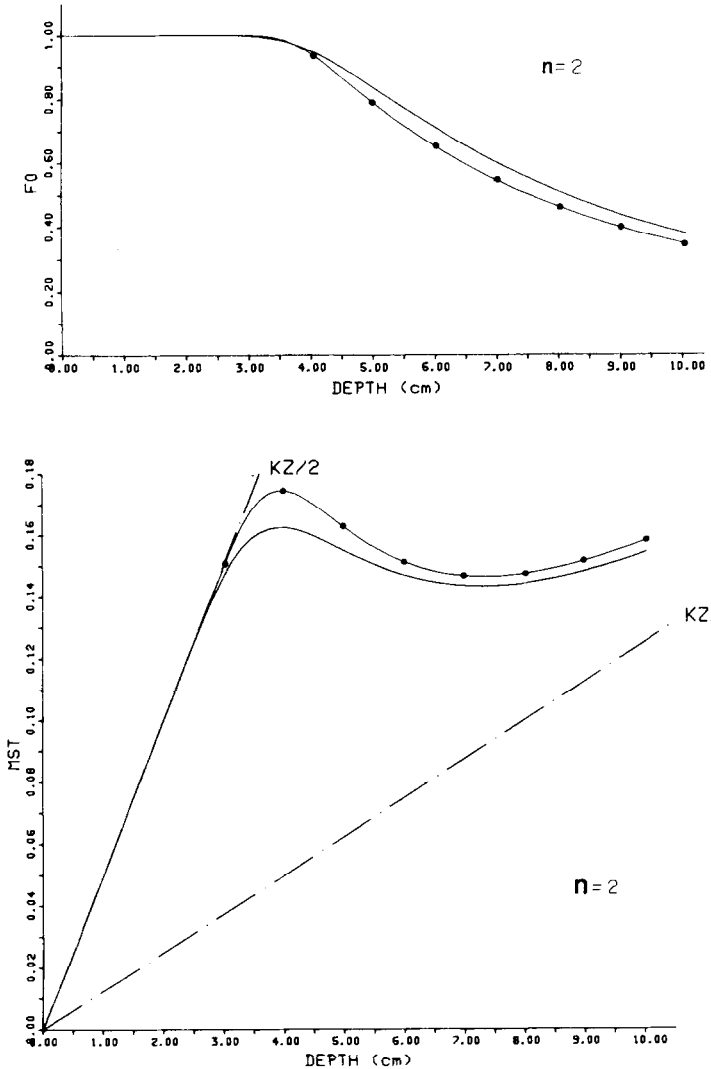

FIG. 3. Planar fluence distribution F_0 and mean square deviation σ^2 (MST) on the central axis of an electron beam (width in the x-direction, 4 cm; in the y-direction, ∞) impinging on a homogeneous medium. The scattering power $T(z)$ is taken to be a constant for all depths, $K = 0.1$ rad^2 cm^{-1}. This case is not realistic from a physical point of view but it allows an easy comparison to the analytical solution (———) of the Fermi–Eyges equation given in [13]. (•—•) is the numerical result for $n = 2$ and $n = 4$. The two dashed lines are the values of an infinite beam ($\sigma^2 = Kz/2$) and of a pencil beam ($\sigma^2 = Kz/8$), respectively; they form the asymptotes of the curve for a finite beam with constant $T(z)$.

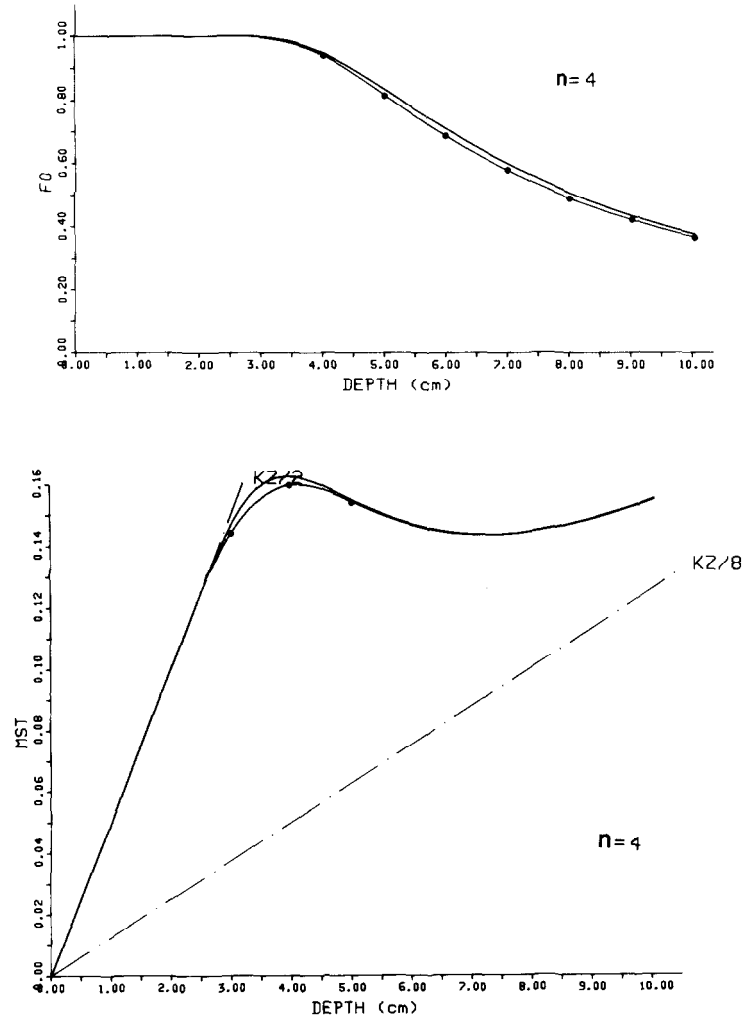

FIG. 3—*Continued*

electrons at that point. The decrease of energy is calculated by using the continuous slowing-down approximation [14]. The isolines are expressed as percentages of the number of electrons per unit surface at $z=0$. The distribution is given for an increasing number of moments. From $n=4$ the pattern of isolines becomes almost stable. Figure 5 shows the distribution for a long cavity ($1 \times 5\ \text{cm}^2$) at a depth of 1 cm in water. In this case the initial electron energy is 20 MeV.

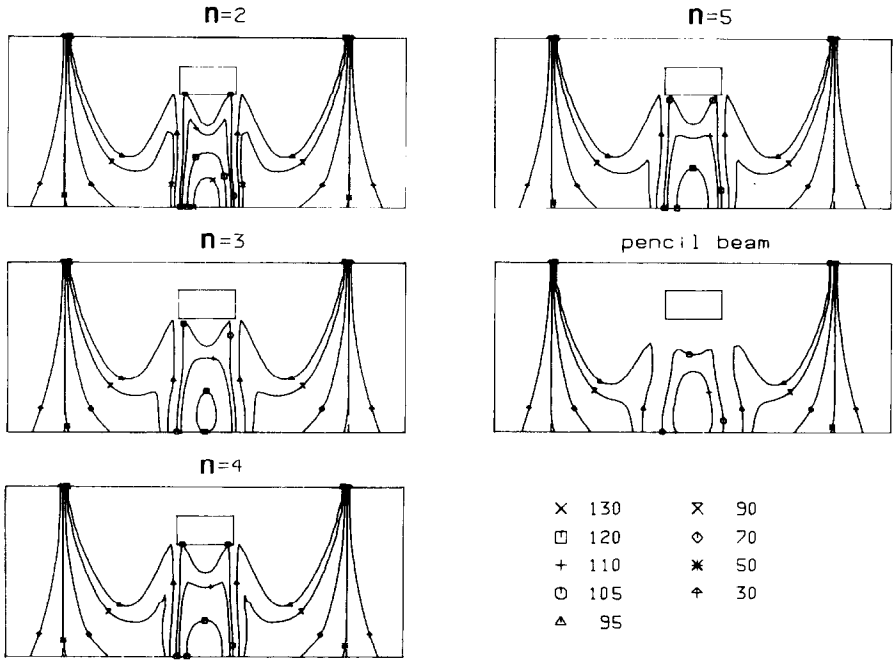

FIG. 4. Planar fluence distribution of a broad beam of width 10 cm crossing an air cavity of cross section 2×1 cm^2 at a depth of 1 cm in water. The initial energy of the electrons is 13 MeV. The isolines are given in percentages of the value at the surface of the medium ($z = 0$). Calculation with the method presented for $n = 2$, 3, 4, and 5 and with the pencil beam method.

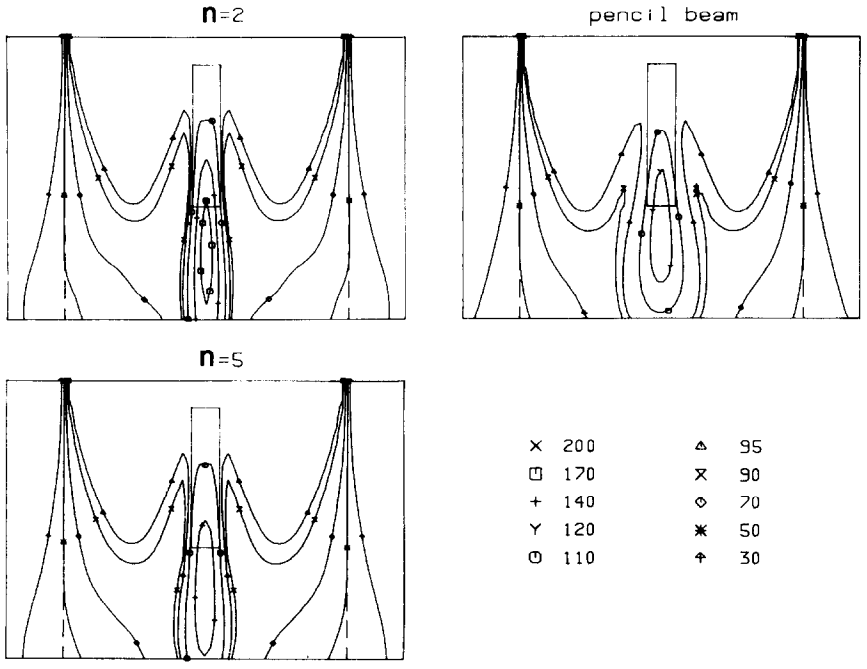

FIG. 5. Planar fluence distribution of a broad beam of width 10 cm crossing an air cavity of cross section 1×5 cm^2 at a depth of 1 cm in water. The initial energy of the electrons is 20 MeV. The isolines are given in percentages of the value at the surface of the medium ($z = 0$). Calculation with the method presented for $n = 2$ and 5 and with the pencil beam method.

7. Conclusion

The results for a homogeneous medium show that the numerical method presented probably converges to the solution of the Fermi–Eyges equation when the number of angular moments is increased. The results for a heterogeneous medium shows a significant influence of the numer of moments up to five or six moments.

The application of this method to the calculation of the therapeutic dose is still in progress. Preliminary results, compared with measured data, have been reported elsewhere [16, 17]. These results have shown that the addition of an adequate calculation of the energy spectrum in each point is important in the case of a heterogeneous medium.

A potential improvment of the numerical method presented is the use of a non-Gaussian scattering function ρ_δ (Eq. (10)) to take large angle scattering and secondary electrons into account.

Appendix A

The shifted Hermite polynomials are defined by

$$\hat{H}_k(\theta; \bar{\theta}, \sigma^2) = \frac{(-1)^k}{G(\theta; \bar{\theta}, \sigma^2)} D^k G(\theta; \bar{\theta}, \sigma^2), \tag{A1}$$

where D^k means $\partial^k/\partial\theta^k$, and

$$G(\theta; \bar{\theta}, \sigma^2) = \frac{1}{\sqrt{2\pi\sigma^2}} \exp\left\{-\frac{(\theta-\bar{\theta})^2}{2\sigma^2}\right\}. \tag{A2}$$

By changing $(\theta-\bar{\theta})/\sqrt{2\sigma^2}$ by t in (A2) we find the relation between the normal Hermite polynomial $H_k(t)$ and the shifted Hermite polynomial:

$$\hat{H}_k(\theta; \bar{\theta}, \sigma^2) = (2\sigma^2)^{-k/2} H_k((\theta-\bar{\theta})/\sqrt{2\sigma^2}). \tag{A3}$$

The $\hat{H}_k$'s fulfill the recursion relation

$$\hat{H}_k = \left(\frac{\theta-\bar{\theta}}{\sigma^2}\right)\hat{H}_{k-1} - \left(\frac{k-1}{\sigma^2}\right)\hat{H}_{k-2}. \tag{A4}$$

Like the normal Hermite polynomials, $\{\hat{H}_k\}$ forms an orthogonal system relative to their weight function $G(\theta; \bar{\theta}, \sigma^2)$:

$$\langle \hat{H}_k, \hat{H}_{k'} \rangle = \int_{-\infty}^{+\infty} \hat{H}_k(\theta)\, \hat{H}_{k'}(\theta)\, G(\theta)\, d\theta$$

$$= 0 \qquad \text{for} \quad k' \neq k \tag{A5a}$$

$$= \frac{k!}{(\sigma^2)^k} \qquad \text{for} \quad k' = k. \tag{A5b}$$

APPENDIX B

In this appendix a number of recurrent relations will be given for the calculation of

$$I_{i,k}(a;\bar{\theta},\sigma^2)=\int_0^a \theta^i \hat{H}_k(\theta;\bar{\theta},\sigma^2)\,G(\theta;\bar{\theta},\sigma^2)\,d\theta \tag{B1}$$

$$\hat{I}_{i,k}(x_1,x_2,b;\bar{\theta},\sigma^2)=\int_{x_1}^{x_2} I_{i,k}\left(\frac{x-b}{\delta};\bar{\theta},\sigma^2\right)dx \tag{B2}$$

$$G_i=\int_{-\infty}^{+\infty}\theta^i G(\theta;\bar{\theta},\sigma^2)\,d\theta. \tag{B3}$$

First, we remark that from definition (A1),

$$\hat{H}_k(\theta;\bar{\theta},\sigma^2)\,G(\theta;\bar{\theta},\sigma^2)=(-1)^k\,D^k G(\theta;\bar{\theta},\sigma^2). \tag{B4}$$

I most cases the recursion relations will be derived by using Eq. (B4) and partial integration.

To compute (B1) consider

$$I_{i,k}(a)=\int_0^a \theta^i(-1)^k\,D^k G(\theta)\,d\theta=-a^i\hat{H}_{k-1}(a)\,G(a)+iI_{i-1,k-1}(a). \tag{B5}$$

For the calculation of (B5) we must consider three cases, $i<k$, $i=k$, and $i>k$, respectively.

For the case $i<k$ we must consider as the starting point of (B5) the term with index $i=0$:

$$I_{0,k-i}(a)=\int_0^a(-1)^{k-i}\,D^{k-i}G(\theta)\,d\theta=-\hat{H}_{k-i-1}(a)\,G(a)+\hat{H}_{k-i-1}(0)\,G(0). \tag{B6}$$

For the case $i=k$ we must consider as the starting point of (B5) the term with indices $i=0$ and $k=0$:

$$I_{0,0}(a)=\int_0^a G(\theta)\,d\theta. \tag{B7}$$

Equation (B7) can be computed further using the error function.

For the case $i>k$ we must consider as the starting point of (B5) the term with index $k=0$,

$$\begin{aligned} I_{i-k,0}(a)&=\int_0^a \theta^{i-k-1}\left(\frac{\theta-\bar{\theta}}{\sigma^2}\sigma^2+\bar{\theta}\right)G(\theta)\,d\theta \\ &=\sigma^2\int_0^a\theta^{i-k-1}\hat{H}_1(\theta)\,G(\theta)\,d\theta+\bar{\theta}\int_0^a\theta^{i-1}G(\theta)\,d\theta \\ &=-\sigma^2a^{i-k}G(a)+(i-k-1)\,\sigma^2I_{i-k-2,0}(a)+\bar{\theta}I_{i-k-1,0}(a). \end{aligned} \tag{B8}$$

The starting points of (B8) are $I_{0,0}(a)$, which is given by (B7) and

$$I_{1,0}(a) = \int_0^a \theta G(\theta)\, d\theta. \tag{B9}$$

To compute (B2) we perform the transformation

$$\int_{x_1}^{x_2} I_{i,k}\left(\frac{x-b}{\delta}; \theta, \sigma^2\right) dx = \int_{(x_1-b)/\delta}^{(x_2-b)/\delta} I_{i,k}(\xi)\, d\xi. \tag{B10}$$

This reduces the problem to the evaluation of

$$\hat{I}_{i,k} = \int_0^a I_{i,k}(\xi)\, d\xi = I_{i,k-1}(a) + i\hat{I}_{i-1,k-1}(a). \tag{B11}$$

For the calculation of (B11), as for the calculation of (B5), we must consider the three cases, $i<k$, $i=k$, and $i>k$, respectively.

For the case $i<k$ we must consider as the starting point of (B11) the term with index $i=0$:

$$\begin{aligned}\hat{I}_{0,k-1}(a) &= \int_0^a -\hat{H}_{k-i-1}(\xi)\, G(\xi)\, d\xi + \int_0^a \hat{H}_{k-i-1}(0)\, G(0)\, d\xi \\ &= -I_{0,k-i-1}(a) + a\hat{H}_{k-i-1}(0)\, G(0).\end{aligned} \tag{B12}$$

For the case $i=k$ we must consider as the starting point of (B11) the term with indices $i=0$ and $k=0$:

$$\hat{I}_{0,0}(a) = \int_0^a I_{0,0}(\xi)\, d\xi = \int_0^a \int_0^\xi G(\theta)\, d\theta\, d\xi. \tag{B13}$$

Equation (B13) can be computed further using the error function and the relation

$$\int \operatorname{erf}\{x\}\, dx = x \operatorname{erf}\{x\} + \frac{1}{\sqrt{\pi}} e^{-x^2}. \tag{B14}$$

For the case $i>k$ we must consider as the starting point of (B11) the term with index $k=0$:

$$\begin{aligned}\hat{I}_{i-k,0}(a) &= \int_0^a I_{i-k,0}(\xi)\, d\xi \\ &= -\sigma^2 I_{i-k,0}(a) + (i-k-1)\,\sigma^2 \hat{I}_{i-k-2,0}(a) + \theta\hat{I}_{i-k-1,0}(a).\end{aligned} \tag{B15}$$

The initial values of (B15) are $\hat{I}_{0,0}(a)$ and $\hat{I}_{1,0}(a)$, which are given by (B13) and

$$\hat{I}_{1,0}(a) = \int_0^a I_{1,0}(\xi)\, d\xi = \int_0^a \int_0^\xi \theta G(\theta)\, d\theta\, d\xi. \tag{B16}$$

The expression (B3) can be calculated by partial integration,

$$G_i = \sigma^2(i-1)\, G_{i-2} + \bar{\theta} G_{i-1}, \tag{B17}$$

for which the first two terms are

$$G_0 = 1 \tag{B18}$$

and

$$G_1 = \bar{\theta}. \tag{B19}$$

Appendix C

In the 3-dimensional case, the distribution F is a function of the depth z, the place in the xy-plane, $r = (x, y)$, and the direction, $\omega = (\theta_x, \theta_y)$. The transfer equation (9) then becomes

$$F(z+\delta, r, \omega) = \int_{\Omega} F(z, r-\delta\omega, \omega')\, \rho_\delta(\omega' \to \omega)\, d\omega', \tag{C1}$$

where

$$\rho_\delta(\omega' \to \omega) = \frac{1}{\pi T\delta} \exp\left\{-\frac{(\theta_x - \theta'_x)^2}{T\delta}\right\} \exp\left\{-\frac{(\theta_y - \theta'_y)^2}{T\delta}\right\}. \tag{C2}$$

In the 3-dimensional case, the distribution F will be approximated by

$$F(z, r, \omega) = \sum_{k=0}^{n} \sum_{k'=0}^{n} a_{kk'} \hat{H}_{kk'}(\omega; \bar{\omega}, \sigma^2)\, G(\omega; \bar{\omega}, \sigma^2), \tag{C3}$$

where $a_{kk'}$, $\bar{\omega}$, and σ^2 are functions of z and r. The functions $G(\omega; \bar{\omega}, \sigma^2)$ is in this case a 2-dimensional Gaussian,

$$\begin{aligned} G(\omega; \bar{\omega}, \sigma^2) &= \frac{1}{2\pi\sigma^2} \exp\left\{-\frac{(\theta_x - \bar{\theta}_x)^2}{2\sigma^2}\right\} \exp\left\{-\frac{(\theta_y - \bar{\theta}_y)^2}{2\sigma^2}\right\} \\ &= G(\theta_x; \bar{\theta}_x, \sigma^2)\, G(\theta_y; \bar{\theta}_y, \sigma^2), \end{aligned} \tag{C4}$$

and the polynomial $\hat{H}_{kk'}(\omega; \bar{\omega}, \sigma^2)$ is the product of two Hermite polynomials,

$$\begin{aligned} \hat{H}_{kk'}(\omega; \bar{\omega}, \sigma^2) &= \frac{(-1)^{k+k'}}{G(\omega; \bar{\omega}, \sigma^2)} D^k_{\theta_x} D^{k'}_{\theta_y} G(\omega; \bar{\omega}, \sigma^2) \\ &= \hat{H}_k(\theta_x; \bar{\theta}_x, \sigma^2)\, \hat{H}_{k'}(\theta_y; \bar{\theta}_y, \sigma^2). \end{aligned} \tag{C5}$$

The directional moments are given by

$$F_{ii'}(z, r) = \int_{-\infty}^{+\infty} \int_{-\infty}^{+\infty} \theta_x^i \theta_y^{i'} F(z, r, \theta_x, \theta_y)\, d\theta_x\, d\theta_y. \tag{C6}$$

Because of the separability of the functions used in the approximation (C2), the algebra used in Section 3 can also be applied in the 3-dimensional case. For example, the relation between the moments F_{ii} and the coefficients a_{kk} will become

$$F_{ii'} = \sum_{k=1}^{i} \sum_{k'=1}^{i} \frac{i!}{(i-k)!} \frac{i'!}{(i'-k')!} G_{i-k}(\bar{\theta}_x, \sigma^2)\, G_{i'-k'}(\bar{\theta}_y, \sigma^2)\, a_{kk'}. \tag{C7}$$

ACKNOWLEDGMENTS

The authors are grateful to Dr. H. Huizenga, Rotterdam Radiation Therapy Institute, and Professor A. J. Hermans, Delft University of Technology, for valuable discussions during the development of the algorithm, and also to H. F. M. Corstens, Delft University of Technology, for reading and discussing the manuscript. This work was supported by a grant of the Queen Wilhelmina Fund for Cancer Research.

REFERENCES

1. K. R. HOGSTROM, M. D. MILLS, AND P. R. ALMOND, *Phys. Med. Biol.* **26**, 445 (1981).
2. A. BRAHME, I. LAX, AND P. ANDREO, *Acta Radiol. Oncol.* **20**, 147 (1981).
3. I. LAX, *Development of a Generalized Gaussian Model for Absorbed Dose Calculation and Dose Planning in Therapeutic Electron Beams*, Thesis, University of Stockholm, 1986 (unpublished).
4. P. ANDREO AND A. BRAHME, *Radiat. Res.* **100**, 16 (1984).
5. M. J. BERGER AND S. M. SELTZER, NBSIR 82-2451, 1982.
6. B. ROSSI AND K. GREISEN, *Rev. Mod. Phys.* **13**, 262 (1941).
7. L. EYGES, *Phys. Rev.* **74**, 1534 (1948).
8. K. R. HOGSTROM AND P. R. ALMOND, *Acta Radiol. (Suppl.)* **364**, 89 (1983).
9. I. LAX, *Radiother. Oncol.* **10**, 307 (1987).
10. A. BRAHME AND B. NILSSON, in *Proceedings, 8th International Conference on the Use of Computers in Radiation Therapy, Toronto 1984* (IEEE Computer Society Press, New York, 1984), p. 157.
11. K. R. SHORTT, C. K. ROSS, A. F. BIELAJEW, AND D. W. O. ROGERS, *Phys. Med. Biol.* **31**, 235 (1986).
12. I. LAX, *Phys. Med. Biol.* **31**, 879 (1986).
13. P. STORCHI AND H. HUIZENGA, *Phys. Med. Biol.* **30**, 467 (1985).
14. International Commission on Radiation Units and Measurements: ICRU Report 35 (ICRU Publ., Bethesda, MD, 1984).
15. D. JETTE, *Med. Phys.* **10**, 141 (1983).
16. P. STORCHI AND H. HUIZENGA, *Med. Phys.* **13**, 581 (1986).
17. A. S. SHUI AND K. R. HOGSTROM, in *Proceedings, 9th International Conference on the Use of Computers in Radiation Therapy, Scheveningen, The Netherlands, 1987*, edited by I. A. D. Bruinvis (Elsevier Science, New York, 1987), p. 69.